Journal of Terramechanics, Volume 48, Issue 4, August 2011, Pages 285-295

Theoretical Analysis of the Spatial Variability in Tillage Forces for Fatigue Analysis of Tillage Machines

A. Abo Al-kheer[1*]; M. Eid[2]; Y. Aoues[2]; A. El-Hami[2]; M. G. Kharmanda[3]; A. M. Mouazen[4]

1- Agricultural Engineering Department, Aleppo University, Syria

2- Rouen Mechanics Laboratory, National Institute of Applied Sciences, France

3- Faculty of Mechanical Engineering, Aleppo University, Syria

4- Environmental Science and Technology Department, Cranfield University, MK43 0AL, United Kingdom

* Corresponding author: Tel: 0096323211410, E-mail: a.aboalkheer@hotmail.com

Address: Agricultural Engineering Department - BP 49, Faculty of Agronomy, Aleppo University, Syria

Abstract

This paper presents a new theoretical model to describe the spatial variability in tillage forces for the purpose of fatigue analysis of tillage machines. The proposed model took into account both the variability in tillage system parameters (soil engineering properties, tool design parameters and operational conditions) and the cyclic effects of mechanical behaviour of the soil during failure ahead of tillage tools on the spatial variability in tillage forces. The stress-based fatigue life approach was used to determine the life time of tillage machines, based on the fact that the applied stress on tillage machines is primarily within the elastic range of the material. Stress cycles with their mean values and amplitudes were determined by the rainflow algorithm. The damage friction caused by each cycle of stress was computed according to the Soderberg criterion and the total damage was calculated by the Miner's law.

The proposed model was applied to determine the spatial variability in tillage forces on the shank of a chisel plough. The equivalent stress history resulted from these forces were calculated by means of a finite element model and the Von misses criterion. The histograms of mean stress and stress amplitude obtained by the rainflow algorithm showed significant dispersions. Although the equivalent stress is smaller than the yield stress of the material, the failure by fatigue will occur after a certain travel distance. The expected distance to failure was found to be $= 0.825 \times 10$. It is concluded that the spatial variability in tillage forces has significant effect on the life time of tillage machines and should be considered in the design analysis of tillage machines to predict the life time. Further investigations are required to correlate the results achieved by the proposed model with field tests and to validate the proposed assumptions to model the spatial variability in tillage forces.

Keywords: spatial variability; tillage forces; tillage machines; fatigue analysis; life time.

1- Introduction

Mechanical loads on tillage machines show considerable variability due to the variability in tillage system parameters and the mechanical behaviour of soil during failure. The variability in tillage system parameters reflects the variability in soil engineering properties and the variations in tool design parameters and operational conditions. The variability in soil engineering properties is resulted from the heterogeneity of agricultural soils. The variations in tool design parameters are due to the manufacturing processes, while the variations in operational conditions are due to the fact that these parameters are not completely controlled during tillage operation.

The crescent manner of soil failure for wide and narrow tines with depth/width ratio less than 5 tend to push the soil upward and forward [1]. This failure pattern involves the development of successive shear planes in front and at the side of tillage tools, which leads to distinct soil failure

blocks (crescents) as the tine moves forward through the soil. The repeated formation of soil crescents creates cyclic loading on the tillage tool. Stafford [2] identified two types of soil failure, namely the brittle failure and the flow failure. Rajaram and Erbach [3] reported the following four soil failure patterns: 1) collapse failure, 2) fracture failure, 3) chip-forming failure and 4) plastic and frictional flow failures. However, they attributed the changes of soil failure patterns to two main factors: the soil type and the moisture content. In other work, Rajaram and Erbach [4] reported that the variations in soil failure patterns are mostly affected by the soil moisture content, soil type, tillage implement type and tillage speed. Factors controlling the soil mechanical behaviour during failure under load are not completely understood/known. In addition, there are no available models that can estimate the effects of soil failure on tillage forces.

Several analytical (e.g. McKyes and Ali [5]; Grisso et al. [6]) and numerical models (e.g. Shen and Kushwaha [7]; Mouazen and Neményi [8]) of soil-tool interaction have been developed to predict tillage forces for assigned tillage system parameters. Furthermore, the effects of tillage system parameters on tillage forces have been investigated [1,9]. Although, these models have shown good agreements with experimental observations for specific test conditions, there is still no well-defined, generalised theoretical model to predict the behaviour of soil-tool interactions [10]. In order to take into consideration the fact that tillage system parameters are variable during tillage operations, Abo Al-kheer et al. [11] proposed a methodology for modeling the variability in tillage forces derived from the variability in tillage system parameters. In another report, they integrated this variability into the reliability analysis for achieving reliable tillage machines [12].

The variability in tillage forces due to the soil failure has been observed in many works in the literature. James and Shrini [13] reported that the large variations in the horizontal force on a plough can be attributed to two factors. These are related to the soil failure and to the within-field spatial variability in soil properties. They confirmed that both of these factors lead to relatively large changes in the horizontal force within a short time period. Makanga et al. [14] studied the

effects of the tine rake angle and the aspect ratio in a laboratory glass-sided soil bin with a dry compacted loam soil with 5.2 % (d.b.) moisture content. They concluded that the horizontal and vertical soil reactions under dry soil conditions were cyclic in nature and in phase. The cyclic variations in the soil reactions were due to the soil failure patterns being repetitive and cyclic in nature throughout the tine travel. Due to variability in soil properties and operational conditions the frequency and amplitude of these cycles vary significantly.

Form a fatigue analysis viewpoint, it is essential to account for the effects of the variability in tillage forces on the resulted stress on tillage machines. The current state of knowledge suggests that there are only experimental works available to estimate the spatial variability in tillage forces [15,16,17]. These methods do not provide a tool for estimating the life time of tillage tools due to fatigue as it cannot account for all affecting parameters.

The main objective of this work is to propose a model for estimating the variability in tillage forces for the purpose of fatigue analysis of tillage machines. The proposed model is applied to estimate the spatial variability in tillage forces on the shank of a chisel plough and the expected distance to failure is calculated. This model is presented in the first part of this work. The second part presents the stress-based fatigue life approach used to estimate the life time of tillage machines.

2- Materials and methods

2-1 Modeling the spatial variability of tillage forces

2-1-1 Basic assumptions for the proposed model

The basic assumptions behind the proposed model are that 1) the spatial variability of tillage forces derived from the variability in tillage system parameters is random, reflecting the heterogeneity in agricultural soils, the uncontrolled field operational conditions during tillage and

97 the manufacturing tolerances of tool design parameters and 2) the spatial variability of tillage
98 forces derived from the mechanical behavior of soil failure is cyclic, reflecting the repeated
99 formation of soil crescents in front of the tool. In addition, we suppose that the total tillage force
100 is the sum of two types of forces, namely the global tillage force and the local tillage force. The
101 global tillage force is due to the tillage system parameters (soil engineering properties, tool design
102 parameters and operational conditions) and the local tillage force is due to the soil failure of
103 cyclic nature.

104 Conventionally, a tillage force is determined by its horizontal and vertical components.
105 Therefore, the horizontal and vertical forces can be calculated, according the earlier assumption,
106 by Equations (1) and (2).

$$= \quad + \tag{1}$$

$$= \quad + \tag{2}$$

107 where is the global horizontal force in kN, is the local horizontal force in kN, is the
108 global vertical force in kN and is the local vertical force in kN.

109 The variability in the global tillage forces (,) can be modelled using the methodology
110 proposed by Abo Al-kheer et al. [11]. This methodology is based on the estimation of tillage
111 forces according to the McKyes-Ali model accounting for the variability in tillage system
112 parameters. Abo Al-kheer et al. [11] subdivided the tillage system parameters contributing to the
113 global tillage forces into three main categories: 1) soil engineering properties including soil bulk
114 density, soil cohesion, internal friction angle, soil-metal friction angle and soil-tool adhesion), 2)
115 tool design parameters including tool width and rake angle and 3) operational conditions
116 including tool working depth, surcharge pressure and tool speed. A combination of graphical and
117 quantitative techniques was proposed for modeling the variability in soil engineering properties
118 and two statistical tests were used to select the probability distributions of these properties,

119 namely the chi-square test and the Kolmogorov-Smirnov test. A total of 57 variations of soil
120 engineering properties, representing 57 different soil samples were considered for implementing
121 our mixed technique approach [11]. The probabilistic characteristics of these properties are given
122 in Table 1.

123 The local tillage forces (,) have been observed in many works in the literature but there
124 are no available models can be used to estimate these forces. However, the majority of reports are
125 attributing these forces to nearly the same parameters contributing to the global tillage forces [4].
126 Therefore, we assume that the local tillage force components can be estimated as a percentage of
127 the global tillage force components as shown in Equations (3) and (4).

$$= \quad . \tag{3}$$

$$= \quad . \tag{4}$$

128 where is the percentage of the local tillage force to the global tillage force. According to the
129 assumptions in Equations 3 and 4 global and local forces are related by the tillage system
130 parameters (soil engineering properties, tool design parameters and operational conditions). The
131 high values of corresponding to a brittle soil failure and the little values of corresponding to a
132 flow soil failure. In other words, the values of the local tillage forces (,) are important for
133 the brittle soil failure since the force cyclic pattern is much more pronounced that with flow
134 failure, while the values of these forces are nearly zero when the soil failure is of flow type [10].

135 The linear correlation between the global and local tillage forces may not be accurate for all soil
136 texture types and all operational conditions. Thus, more work should be done to investigate the
137 relationship between the global and local tillage forces.

138 Based on the earlier assumptions, the spatial variability in tillage forces can be represented by the
139 spatial variability in the global and local tillage forces, as shown in Equations (5) and (6).

$$( ) = \quad ( ) + \quad ( ) \tag{5}$$

$$( ) = \quad ( ) + \quad ( ) \tag{6}$$

where represents the spatial variability in the global horizontal force in kN, represents the spatial variability in the local horizontal force in kN, represents the spatial variability in the global vertical force in kN, represents the spatial variability in the local vertical force in kN and is the distance travelled in .

2-1-2 Modeling the spatial variability in the global tillage forces

The spatial variability in the global tillage forces (,) is resulted from the spatial variability of soil resistance and uncontrolled operational conditions. This spatial variability can be attributed to several factors, e.g., the characteristics of the field, the geography and topography of the field and the soil management system (no-till, reduced till or conventional tillage). Therefore, the spatial variability in the global tillage forces changes from one location to another within the same field and from field to field.

To take the earlier observations into account, we modelled the spatial variability in the global tillage forces with the following assumptions: 1) the spatial variability in the global tillage forces is linear and 2) the distance between two successive changes of the values of global tillage forces is random. The linearity of the spatial variability in the global tillage forces between the global tillage force samples may not be an accurate assumption. However, the increase of the global tillage force samples improves the accuracy of this model. Taking the distance as a random variable allows considering the variability in the field characteristics over the distance . Based on these assumptions, the spatial variability in the global tillage forces can be expressed as in Equations (7) and (8). An illustration of the spatial variability in the global tillage forces over the distance is shown in Figure 1.

$$( ) = \quad ( ) + \quad (+ 1) - \quad ( ) \frac{- \sum \quad ( )}{( )} \qquad = 1, \dots , \qquad (7)$$

$$( ) = \quad ( ) + \quad (+ 1) - \quad ( ) \frac{- \sum \quad ( )}{( )} \qquad = 1, \dots , \qquad (8)$$

where ( ) is the i*th* global horizontal force sample in kN, ( ) is the i*th* global vertical force sample in kN, is the distance between two successive changes of the global tillage force values in , ∑ ( ) is the cumulative sum of ( ) for = 1 to − 1 and is the number of the global tillage force samples.

2-1-3 Modeling the spatial variability in the local tillage forces

As mentioned before, the soil failure creates cyclic loading on tillage tools by the repeated formation of soil crescents. The global tillage forces are calculated at failure when the tillage forces achieve their maximum values. The local tillage forces reach their maximum values at failure and then drop down after the first soil block has formed and these forces will increase to form the second soil block until achieve failure and so on. Therefore, we can imagine that the total tillage forces fluctuate below the global tillage forces.

Based on the fact that the effect of the soil failure in the tillage forces is cyclic, the sinusoid function was used to describe the spatial variability in the local tillage forces with the amplitude and cycle length . Therefore, the spatial variability of tillage forces can be expressed as in Equations (9) and (10) and illustrated as in Figure 2. The terms − ( ) and − ( ) are added to these Equations to keep the values of total tillage forces fluctuate below the values of global tillage forces.

$$( ) = \quad ( ) \sin \quad 2 \quad \frac{- \sum \quad ( ) - \sum \quad ( )}{( )} \quad - \quad ( ) \quad = 1, \dots , \tag{9}$$

$$( ) = \quad ( ) \sin \quad 2 \quad \frac{- \sum \quad ( ) - \sum \quad ( )}{( )} \quad - \quad ( ) \quad = 1, \dots , \tag{10}$$

where ( ) is the j*th* local horizontal force in kN, ( ) is the j*th* local vertical force in kN, ( ) is the cycle length of the j*th* cycle in , is the number of calculated values in a cycle and is the number of cycles between two successive changes of the global tillage forces.

2-1-4 Modeling the spatial variability in the total tillage forces

By combining the spatial variability in the global and local tillage forces and taking into account the assumption that the local tillage force components can be estimated as a percentage of the global tillage force components, it concluded that the spatial variability in tillage forces can be represented by the following five parameters:

$$(\ ) = \ (P_{HG}, S_1, S_2, \ ) \tag{11}$$

$$(\ ) = \ (P_{VG}, S_1, S_2, \ ) \tag{12}$$

All of these parameters can be considered as variables to represent the variability in the forces on the tillage tool during the tillage operation, as shown in Figure 3.

2-1-5 Special cases

Two special cases of spatial variability in tillage forces, namely, at constant global tillage forces and at insignificant local tillage forces are shown in Figures 4 and 5, respectively. The first case supposes that all tillage system parameters do not vary during tillage. This assumption may be suitable for quasi-homogeneous soils and when the variations in the operational conditions are not important. The second case can be used to represent the spatial variability in tillage forces when the soil failure is of flow type. However, in most cases, both the global and local tillage forces should be taken into consideration in the estimation of the spatial variability in tillage forces.

2-2 **Stress-based fatigue life**

The stress-based fatigue life approach is generally characterized by a high-cycle fatigue methodology, and is widely used in design applications where the applied stress is primarily within the elastic range of the material and the resulting fatigue life is long. The basis of the

stress-based fatigue life approach is the stress (S)-number of cycles to failure (N) curve, also known as a Wöhler curve. The S-N curve is a graph of the amplitude of a cyclical stress against the logarithmic scale of cycles to failure. In some materials, particularly ferrous alloys, the S-N curve flattens out eventually, so that below a certain limit, called the fatigue limit or the endurance limit (typically > 10 cycles), the material may not fail and can be cycled infinitely [18] (curve a in Figure 6). For some other materials such as aluminum and copper alloys, no fatigue limit exists. In such cases, the fatigue strength for a given number of cycles (e.g. 1×10 cycles) must be specified [19] (curve b in Figure 6).

The S-N curve for a material, that has a fatigue limit such as steel, can be expressed as in Equation (13).

$$= \cdot \quad \begin{matrix} < \\ \geq \end{matrix} \tag{13}$$

where is the stress amplitude in MPa, is the regression intercept (also called the fatigue strength coefficient) in MPa, is the regression slope (also called the fatigue strength exponent), is the number of cycles and is the number of cycles corresponding to the fatigue limit .

The most basic S-N curves are generated using a fully-reversed stress, where the ratio (R) between the maximum and minimum stress is equal to -1. When the stress applied on a structure is constant over the structure life and the ratio (R) is equal to -1, the Equation (13) can be used directly to determine the number of cycles to failure i.e. the fatigue life. If the number of cycles to failure is greater than the number of cycles corresponding to the fatigue limit , it can be accepted that the structure has an infinite life.

When the ratio R is not equal to -1, a Haigh diagram is usually used to estimate the fatigue life. This diagram plots the mean stress along the x-axis and the stress amplitude along the y-axis and the lines of constant life are drawn through the data points. A very substantial amount of testing is required to generate a Haigh diagram, and it is usually impractical to develop curves for all

225 combinations of mean and amplitude stresses. Therefore, several empirical criteria that relate the
226 stress amplitude to the mean stress have been developed to address this difficulty. These criteria
227 define various curves to connect the fatigue limit on the stress amplitude axis to either the yield
228 strength or the ultimate strength on the mean stress axis [20]. The zone under the curves defined
229 the safe zone against fatigue while the zone above the curves represents the failure zone. Figure 7
230 illustrates three of these criteria, namely the criterions of Goodman, Gerber and Soderberg.

231 Kwofie [21] proposed a function, presented in Equation (14), to take into account the effect of
232 mean stress. This function allows determining the stress amplitude according to the material
233 constant, material properties, number of cycles to failure and to different fatigue criteria.

$$= \quad 1 - \quad \text{—} \tag{14}$$

234 where is a numerical constant, representing the mean stress sensitivity of the material, is the
235 mean stress in MPa and is the ultimate strength in MPa. The value of the numerical constant
236 depends on the fatigue criterion (Goodman, Gerber, Soderberg, etc.).

237 In practice, a structure (e.g. tillage machines) is exposed to a random stress. In such cases, the
238 random stress should be reduced to a series of simple cyclic stresses using counting methods, e.g.,
239 range pair method and rainflow method [22]. The rainflow method is the most popular and widely
240 used in practice [23]. It allows one to determine the amplitude and mean value (,) for each
241 stress cycle at a fixed time interval or a distance interval . The damage friction caused by the
242 i*th* cycle of stress can be computed by Equation (15).

$$= \frac{1}{(\quad , \quad)} \tag{15}$$

243 where (,) is the number of cycles to failure according to the amplitude and the
244 mean value . In this work, the Soderberg criterion was used to determine , based on the

245 fact that the applied stress is primarily within the elastic range of the material. According to this
246 criterion, = [21] and was calculated as in Equation (16).

$$= \frac{}{1 -} \tag{16}$$

247 The total damage, caused by all cycles, can be computed by a cumulative damage model. More
248 than 60 fatigue damage models have been proposed for this purpose. However, the linear damage
249 rule (Miner's law) is still dominantly used because of its simplicity in addition to its sufficient
250 accuracy [24]. For these reasons the Miner's law was used in this work. The Miner's law assumes
251 that the total damage can be expressed as the sum of damage frictions, as shown in Equation (17).
252 Failure is assumed to occur when ≥ 1.

$$= \tag{17}$$

253 where is the number of cycles determined by the rainflow algorithm for the time interval or
254 the distance interval . If the total damage is calculated for a distance interval , which is the
255 case of our work, the expected travel distance to failure can be calculated by dividing the distance
256 interval by the total damage, i.e. = , to fulfill the assumption that the failure will occur
257 when ≥ 1.

258

259 **3- Numerical application**

260 **3-1 Modeling the spatial variability in tillage forces**

261 The proposed model, presented in Section 2.1, is implanted in MATLAB program (Mathworks
262 INC. 2008) to model the spatial variability in tillage forces on the shank of a chisel plough shown
263 in Figure 8. The shank cross-section is rectangular of height $h = 58$ and width $= 32$,
264 as shown in Figure 9.

265 Abo Al-kheer et al. [11] found that the variability in the global horizontal and vertical forces
266 followed lognormal distributions. The distribution parameters of these forces were $= 0.872$,
267 $= 0.449$, $= 0.004$ and $= 0.447$, where and are the scale and shape
268 parameters of a lognormal distribution, respectively. The correlation coefficient between and
269 was found to be $(,) = 0.93$. Therefore, the variability in the local horizontal and
270 vertical forces should have lognormal distributions with the following distribution
271 parameters $= \ln( ) +$, $=$, $= \ln( ) +$ and $=$. In this
272 work, was selected to be equal 0.2 for brittle failure. Furthermore, we assumed
273 that and have normal distributions with the following distribution parameters $=$
274 10, $= 0.1$, $= 0.05$ and $= 0.1$, where and are the location and scale
275 parameters of a normal distribution, respectively. The distribution parameters of the main model
276 parameters, as described in Equations (11) and (12), are listed in Table 2.

277 To generate correlated tillage forces and , two non-correlated normalized variables
278 and were generated by the MATLAB function "normrnd" and then the random values of
279 and were calculated using two transformations [25,26]. The first one transforms non-
280 correlated normalized variables and to correlated normalized variables and and the
281 second one transforms correlated normalized variables to correlated tillage forces and .
282 The spatial variability of the horizontal and vertical forces can then be shown in Figure 10 for a
283 distance of 1000 .

284 From Figure 10, it can be observed that a clear correlation exists in the spatial variability between
285 the horizontal and vertical forces. This is resulted from the correlation between the global
286 horizontal and vertical forces ($(,) = 0.93$). Another observation is the correlation
287 between the global tillage forces (,) and the local tillage forces (,). The increase
288 of global tillage forces increases the amplitudes of local tillage forces and vice-versa. These

289 increases in force amplitudes are marked in cycles in Figure 10. This is caused by the calculation
290 of the local tillage forces as a percentage of the global tillage forces.

291 **3-2 Equivalent stress history**

292 The equivalent stress, resulted from the tillage forces, was calculated according to the Von misses
293 criterion. Firstly, the point of the maximum equivalent stress was determined by means of the
294 finite element (FE) method and ANSYS program (ANSYS INC. V11). Figure 11 shows the
295 meshed model, boundary conditions and the point of maximum equivalent stress (in MPa)
296 determined for the mean values of tillage forces $= 2.641$ and $= 1.106$. Then, the
297 equivalent stress, presented in Figure 12, was calculated at the point of maximum equivalent
298 stress using the finite element model, implemented in the CALFEM toolbox of MATLAB [27].

299 The rainflow algorithm [23] was used to extract the stress cycles with their amplitude and mean
300 values. The histograms of stress amplitude and mean stress are shown in Figure 13. Both the
301 histograms indicate that the dispersions of mean stress and stress amplitude are significant. This
302 reflects the high dispersions of the spatial variability in tillage forces.

303 **3-3 Expected distance to failure**

304 The material constants (the regression intercept and the regression slop) used to calculated the
305 expected distance to failure are a $= 754$ MPa and $= 0.121$. The yield stress of the material
306 is $= 250$ MPa. The total damage was calculated over the distance ($= 980.902$)
307 according to Equation (17). The total damage is equal to $= 1.189 \times 10$. By dividing the
308 distance by the total damage , the expected distance to failure is $= 0.825 \times 10$.
309 Despite the fact that the equivalent stress is smaller than the yield stress (Figure 10), the failure
310 will occur after a certain distance . This example shows the significant effect of the spatial
311 variability in tillage forces on the life time of tillage machines. Since agricultural soils are

312 characterized to be high spatial variability [17], it is expected that this variability will reduce the
313 life time of tillage tools.

314 The expected distance to failure is plotted as a function of the shank cross-section dimensions
315 (, h) in Figure 14. For all combinations of and h, the equivalent stress is smaller than the yield
316 stress. The minimum distance to failure $= 2.004 \times 10$ occurs with $= 25$
317 and $h = 55$, the maximum distance to failure $= 9.213 \times 10$ occurs with
318 $= 35$ and $h = 70$. It is noted that the augmentation of the shank cross-section
319 dimensions increases the distance to failure. This is due to the fact that the augmentation of the
320 shank cross-section dimensions augments the resistance to failure by fatigue and by consequence
321 augments the distance to failure. The Figure 14 allows one determining the shank dimensions
322 according to the required distance to failure, e.g., for $= 10 \times 10$ the shank dimensions
323 are $= 25$ and $h = 65$.

324 To investigate the effect of the percentage of the local tillage forces to the global tillage forces ( )
325 on the expected distance to failure ( ), the percentage is plotted against the logarithmic scale
326 of in Figure 15. It is observed that with an increase of from 01 to 0.4, a reduction of
327 of 1.2×10 will take place, meaning that the reduction of due to the augmentation of is
328 very significant. Indeed, the increase of the value of the percentage augments the amplitudes of
329 the fatigue cycles and as a result reduces the distance to failure (Equations 15, 16 and 17).
330 Therefore, to reduce the values, (by consequence, the values of the local tillage forces) it is
331 recommended to perform the tillage operation when the moisture content is closed to the liquid
332 limits, where the soil conditions became most favorable for soil-working. This can improve
333 significantly the expected distance to failure and by consequence the life time of tillage machines.

334

335

4- Conclusions

A new model to describe the spatial variability in tillage forces and the methods used to calculate the life time of tillage machines are presented in this paper. The proposed model was applied to determine the spatial variability in tillage forces for the shank of a chisel plough and the expected distance to failure was caculated. The expected distance to failure for the shank cross section of $h = 58$ and $= 32$ was found to be $= 0.825 \times 10$. In addition, different values of h and could be used to calculate the expected distance to failure. Based on this work the following conclusions can be drawn:

- The spatial variability in tillage forces can be modelled by only five random parametes (P_{HG}, P_{VG}, S_1, S_2, τ).
- The spatial variability in tillage forces has singificant effect on the equivalent stress history.
- The dispersions of mean stress and stress amplitude of the stress cycles are important.
- The failure by fatigue will occur even the equilvalent stress is smaller than the yield stress of the material.
- The shank cross-section dimensions have a significant impact on the distance to failure ($= 2.004 \times 10$, $= 9.213 \times 10$).
- The effect of the percentage of the local tillage forces to the global tillage forces ( ) on the expected distance to failure ( ) is very significant.

A further research is needed to investigate the relathionships between the global and local tillage forces (P_{HG}, P_{VG}) and the variability in the others parameters (S_1, S_2, τ). In addition, a further study is needed to validate the results achieved in this paper with experiment.

References

[1] R.J. Godwin, A review of the effect of implement geometry on soil failure and implement force, Soil & Tillage Research 97(2007) 331-340.

[2] J.V. Stafford, Force prediction models for brittle and flow failure of soil by draught tillage tool, Journal of Agricultural Engineering Research 29(1984) 51-60.

[3] G. Rajaram, D.C. Erbach, Soil failure by shear versus modification by tillage: A review, Journal of Terramechanics 33(1996) 265-272.

[4] G. Rajaram, D.C. Erbach, Drying stress effect on mechanical behaviour of a clay-loam soil, Soil & Tillage Research 49(1998) 147-158.

[5] E. McKyes, O.S. Ali, The cutting of soil by narrow blades, Journal of Terramechanics 14(1977) 43-58.

[6] R.D. Grisso, J.V. Perumpral, C.S. Desai,.A soil-tool interaction model for narrow tillage tools, No. 80-1518 ASAE, St Joseph, MI, 1980.

[7] J. Shen, R.L. Kushwaha, Quick finite element analysis of soil tool interactions, Computers and Electronics in Agriculture 9(1993) 289-299.

[8] A.M. Mouazen, M. Neményi, Finite element analysis of subsoiler cutting in non-homogeneous sandy loam soil, Soil & Tillage Research 51(1999) 1-15.

[9] R.J. Godwin, M.J. O'Dogherty, C. Saunders, A.T. Balafoutis, A force prediction model for mouldboard ploughs incorporating the effects of soil characteristic properties, plough geometric factors and ploughing speed, Biosystems Engineering 97(2007) 117-129.

[10] H.P.W. Jayasuriya, V.M. Salokhe, A review of soil–tine models for a range of soil, Journal of Agricultural Engineering Research 79(2001) 1-13.

383 [11] A. Abo Al-kheer, M.G. Kharmanda, A. El-hami, Probabilistic analysis of soil tillage forces,
384 Proceedings of the 18th ISTRO Conference, August 2009, Izmir, Turkey.

385 [12] A. Abo Al-kheer, A. El Hami, M.G. Kharmanda, A.M. Mouazen, Reliability-Based Design
386 for Soil Tillage Machines, Journal of Terramechanics 48(2011) 57-64.

387 [13] L.G. James, K.U. Shrini, An improved technique for agricultural implement draught
388 analysis, Soil & Tillage Research 35(1995) 175-182.

389 [14] J.T. Makanga, V.M. Salokhe, D. Gee-Clough, Effects of tine rake angle and aspect ratio on
390 soil reactions in dry loam soil, Journal of Terramechanics 34(1997) 235-250.

391 [15] D. Sirjacobs, B. Hanquet, F. Lebeau, M.F. Destain, On-line soil mechanical resistance
392 mapping and correlation with soil physical properties for precision agriculture, Soil and Tillage
393 Research 64(2002) 231-242.

394 [16] B. Hanquet, D. Sirjacobs, M.F. Destain, Analysis of soil variability measured with a soil
395 strength sensor, Precision Agriculture 5(2004) 227-246.

396 [17] A.M. Mouazen, H. Ramon, Development of on-line measurement system of bulk density
397 based on on-line measured draught, depth and soil moisture content, Soil and Tillage Research
398 86(2006) 218-229.

399 [18] J. Schijve, Fatigue of structures and materials in the 20th century and the state of the art,
400 International Journal of Fatigue 25(2003) 679-702.

401 [19] I. Marines, X. Bin, C. Bathias, An understanding of very high cycle fatigue of metals,
402 International Journal of Fatigue 25(2003) 1101-1107.

403 [20] G.P. Sendeckyj, Constant life diagrams - a historical review, International Journal of Fatigue
404 23(2001) 347-353.

[21] S. Kwofie, An exponential stress function for predicting fatigue strength and life due to mean stresses, International Journal of Fatigue 23(2001) 829–836.

[22] J.A. Bannantine, J.J. Comer, J.L. Handrock, Fundamentals of metal fatigue analysis, Prentice Hall, New Jersey, 1990.

[23] A. Nieslony, Determination off ragments of multiaxial service loading strongly influencing the fatigue of machine components, Mechanical Systems and Signal Processing 23(2009) 2712–2721.

[24] A. Fatemi, L. Yang, Cumulative fatigue damage and life prediction theories: a survey of the state of the art for homogeneous materials, International Journal of Fatigue 20(1998) 9-34.

[25] A. Der Kiureghian, P-L. Liu, Structural reliability under incomplete probability information, Journal of Engineering Mechanics 112(1986) 85-104.

[26] A. Haldar, S. Mahadevan, Probability, reliability, and statistical methods in engineering design, John Wiley & Sons, New York, 2000.

[27] P.E. Austrell, O. Dahlblom, J. Lindemann, A. Olsson, K.G. Olsson, K. Persson, H. Petersson, M. Ristinmaa, G. Sandberg, P.A. Wernberg, CALFEM; A finite element toolbox to MATLAB, Version 3.4, Lund : Structural Mechanics, LTH, Sweden, 2004.

Tables

Table 1: Probabilistic characteristic of soil engineering properties (Abo Al-kheer et al. [11])

Soil engineering properties	Type of distribution	Distribution parameters
Soil density, kN. m	Lognormal	$= 0.13, \quad = 2.7$
Soil cohesion, kPa	Weibull (2P)	$= 15.51, \quad = 1.66$
Internal friction angle, deg	Normal	$= 32, \quad = 3.96$
Soil-tool friction angle, deg	Weibull (3P)	$= -64.08, \quad = 87.14, \quad = 31.52$
Soil-tool adhesion, kPa	Exponential	$= 0.76$

and are the shape and scale parameters of a lognormal distribution; , and are, respectively, the location, scale and shape parameters of a Weibull distribution; , are, respectively, the location and scale parameters of a normal distribution; is the scale parameter of a exponential distribution.

Table 2: Distribution parameters of the model's parameters

Model's parameters	Distribution type	Distribution parameters
[ ]	Lognormal	$= 0.872,$ $= 0.449$
[ ]	Lognormal	$= 0.004,$ $= 0.447$
[ ]	Normal	$= 10,$ $= 1$
[ ]	Normal	$= 50,$ $= 5$
	Deterministic	$= 0.2$

Figures

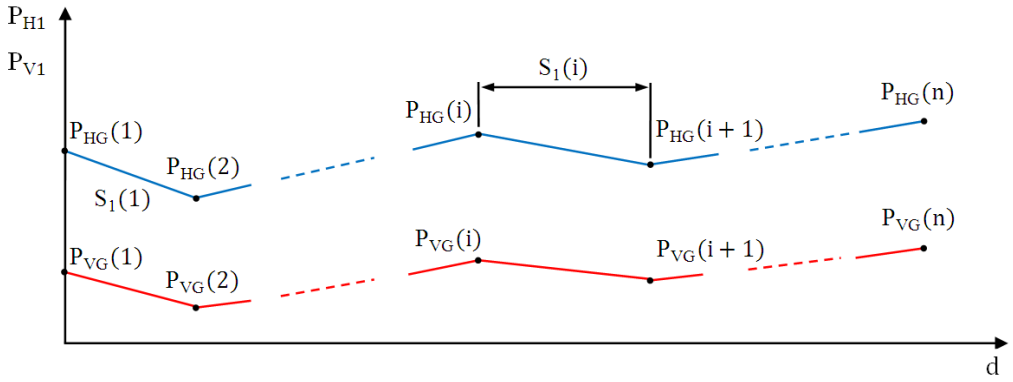

Figure 1: Illustration of the spatial variability in the global tillage forces

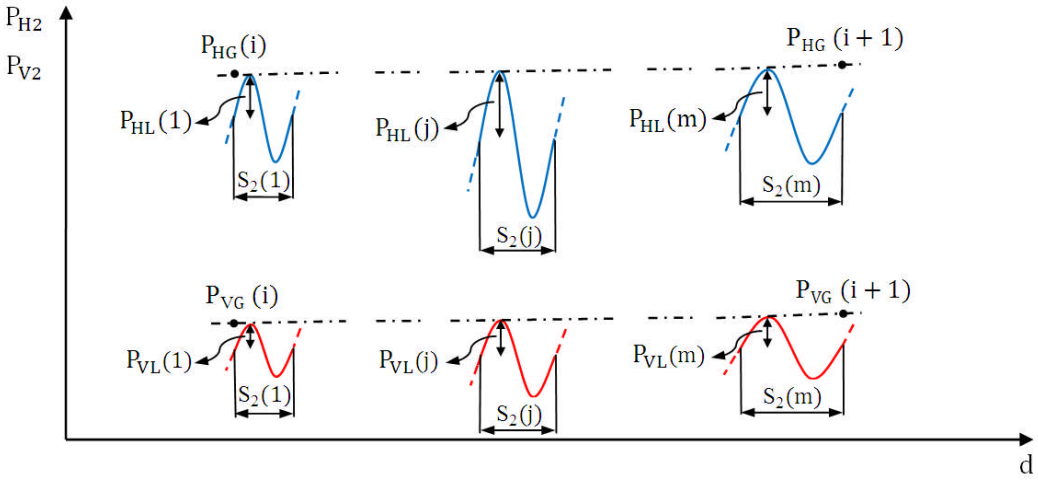

Figure 2: Illustration of the spatial variability in the local tillage forces

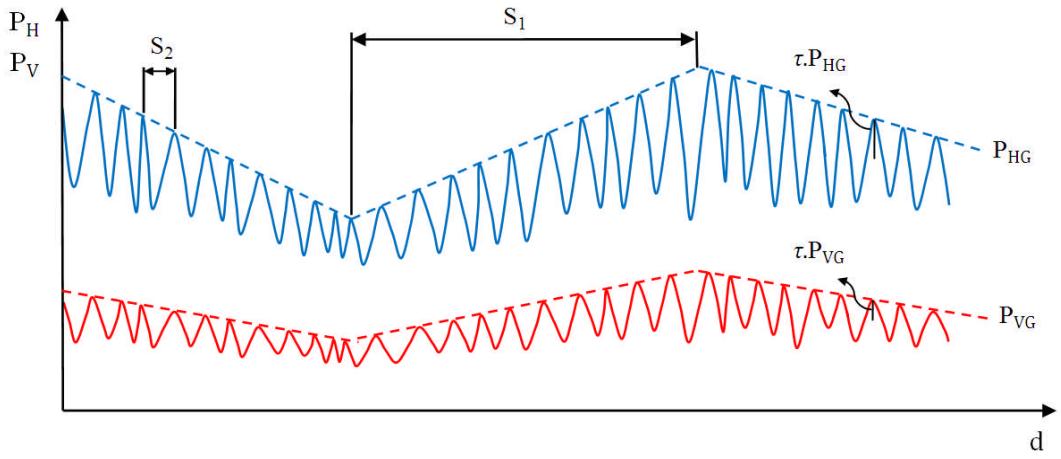

Figure 3: Illustration of the spatial variability in the horizontal and vertical forces

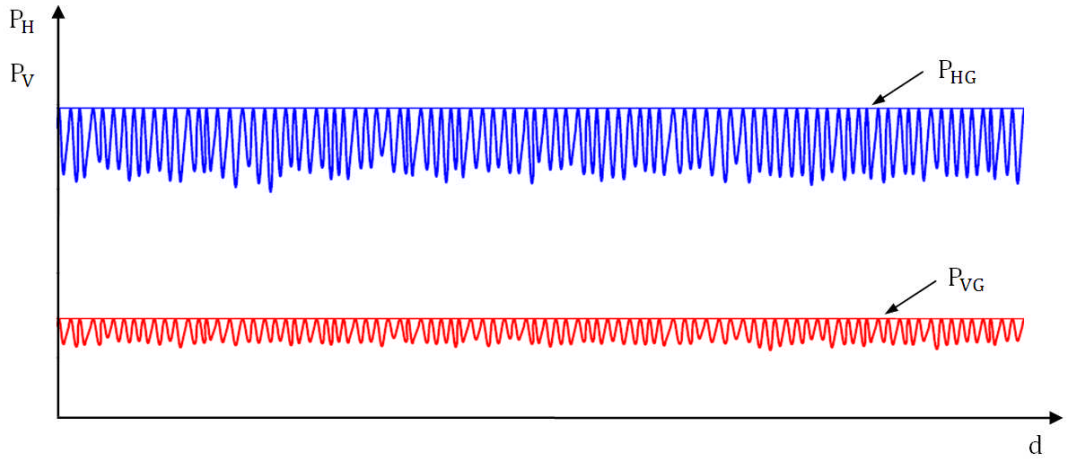

Figure 4: Spatial variability in tillage forces for constant global tillage forces

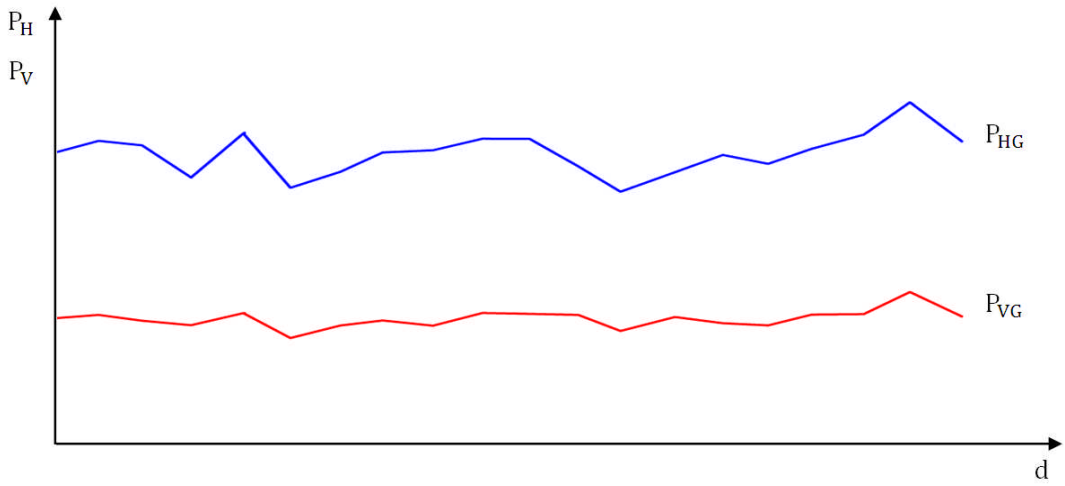

Figure 5: Spatial variability in tillage forces when omitting local tillage forces

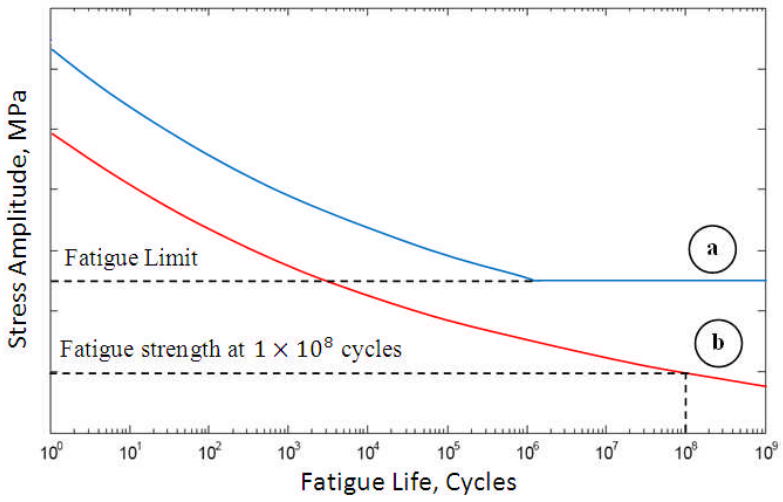

Figure 6: Typical S-N curves

564

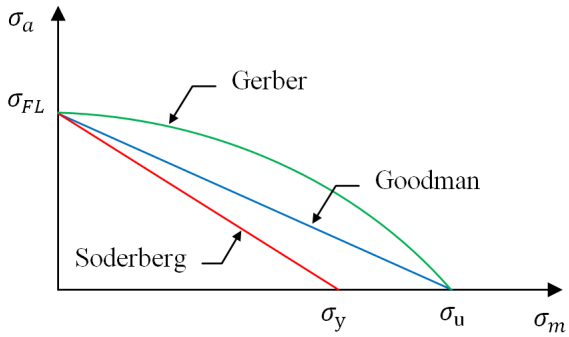

565

566 Figure 7: Comparison of mean stress - stress amplitude relationships

567 (where is the fatigue limit, is the ultimate strength and is the yield strength)

568

569

570

571

572

573

574

575

576

577

578

579

580

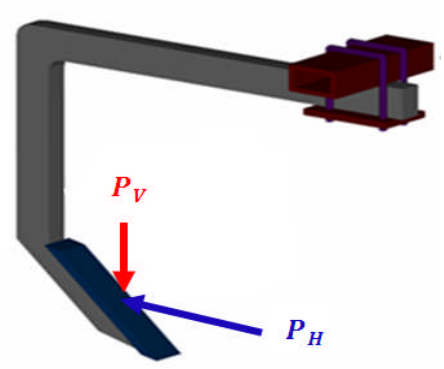

Figure 8: Illustration of the shank of a chisel plough with tillage forces

598

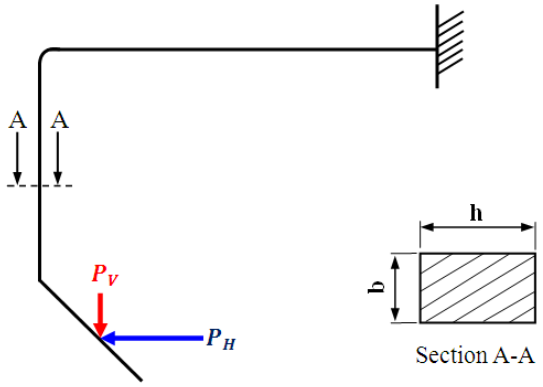

599

600 Figure 9: A schematic drawing of the chisel plough shank ($h = 58$, $= 32$)

601

602

603

604

605

606

607

608

609

610

611

612

613

614

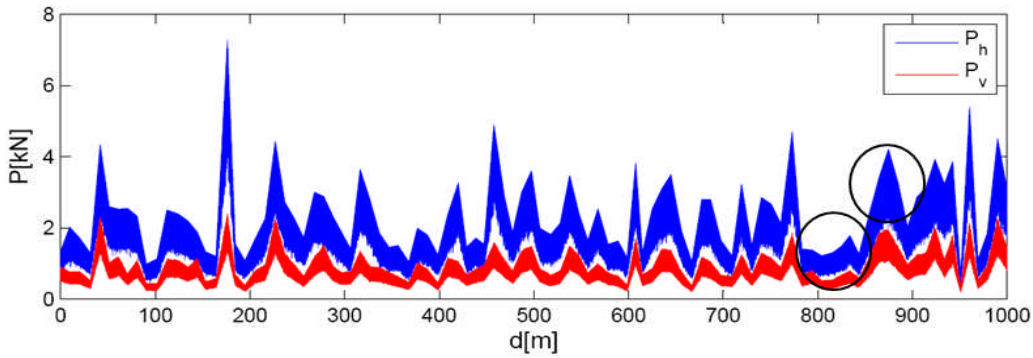

Figure 10: The spatial variability of the horizontal and vertical forces across proposed 1000 m distance

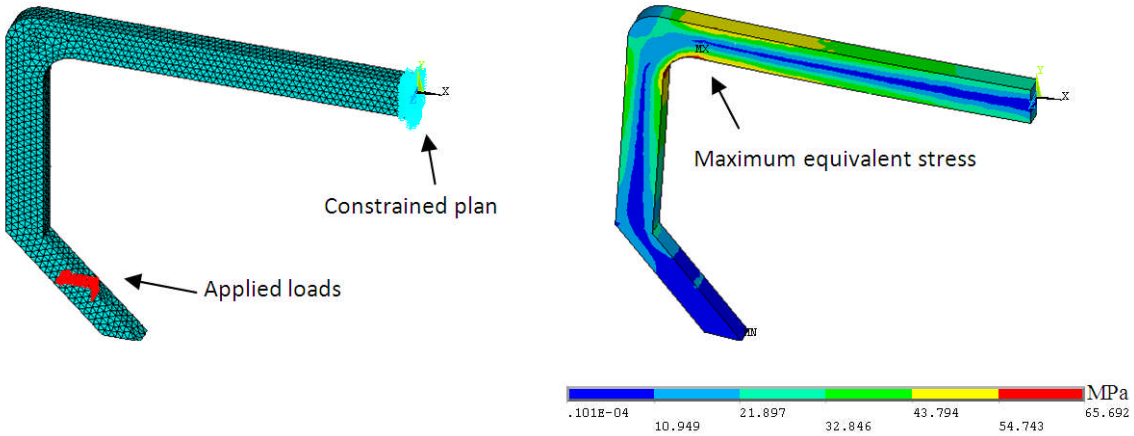

Figure 11: a- Meshed model and boundary conditions; b- Point of maximum equivalent stress

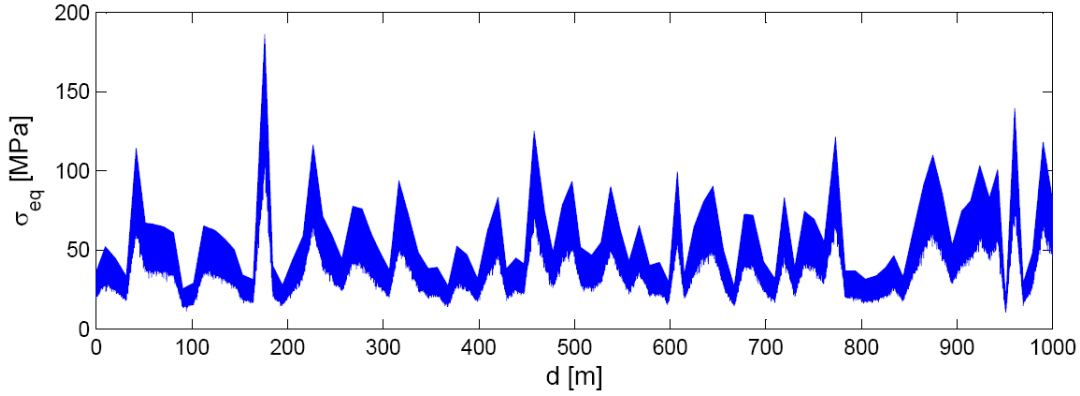

Figure 12: Equivalent stress history across proposed 1000 m distance

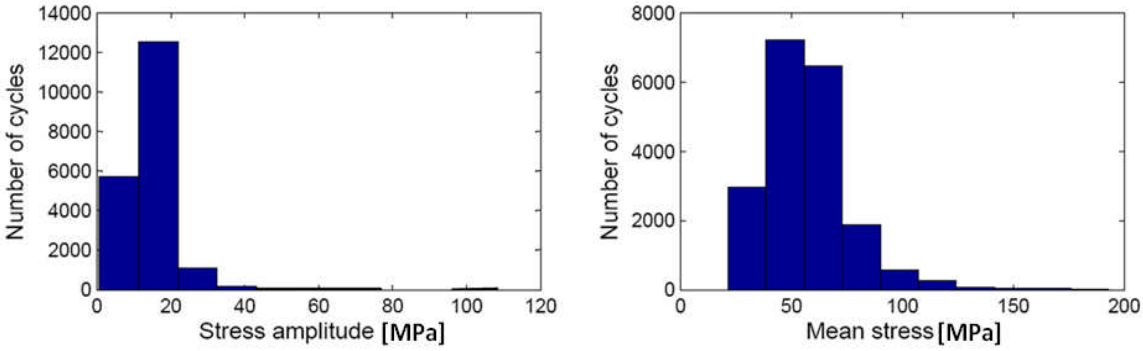

Figure 13: Histograms of stress amplitude and mean stress

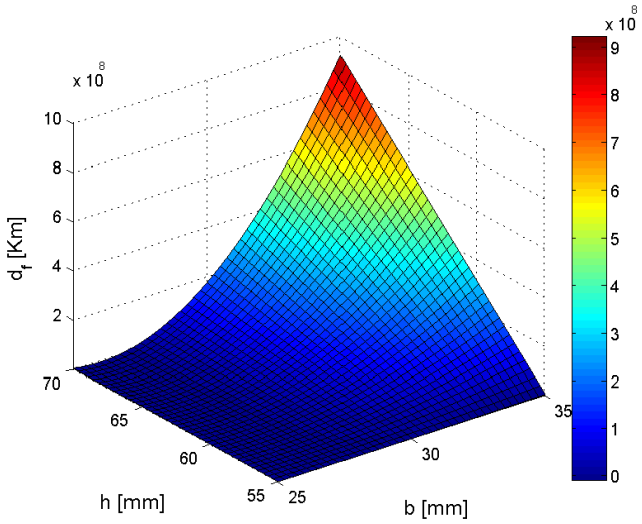

Figure 14: Distance to failure-Shank dimensions plot

694

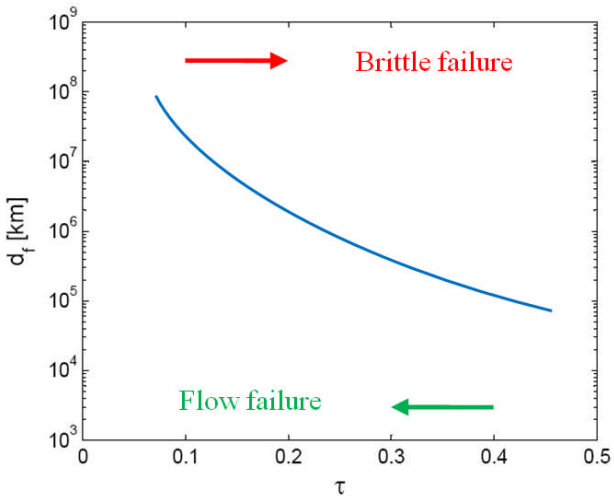

695

696 Figure 15: – relationship

697

698